AD-A033 314 CITY UNIV OF NEW YORK GRADUATE SCHOOL AND UNIV CENTER F/G 13/13
BUCKLING OF A COMPLETE SPHERICAL SHELL UNDER UNIFORM EXTERNAL P--ETC(U)
1976 H E RAUCH, N H JACOBS, J L MARZ AF-AFOSR-2063-71
UNCLASSIFIED AFOSR-TR-76-1219 NL

| OF |
AD
A033314

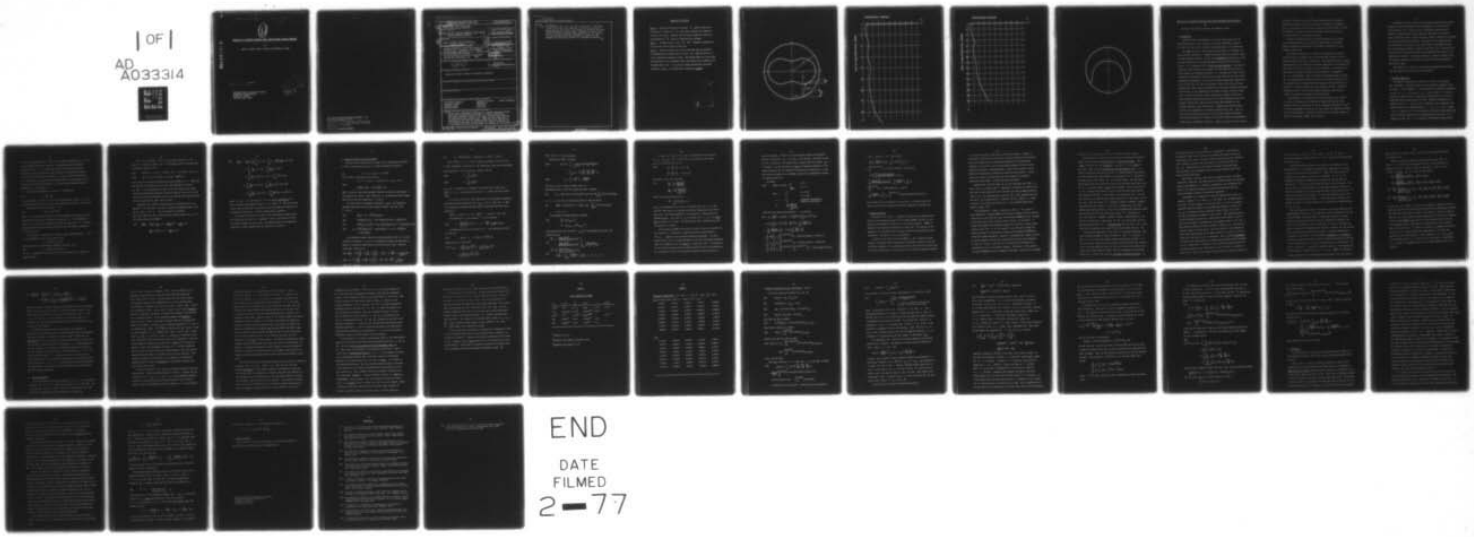

END

DATE
FILMED
2-77

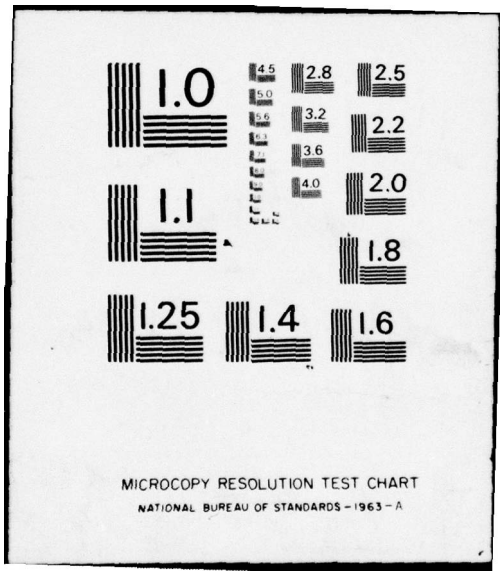
1.0
1.1
1.25
1.4
1.6
1.8
2.0
2.2
2.5
2.8
3.2
3.6
4.0
4.5
5.0
5.6
MICROCOPY RESOLUTION TEST CHART
NATIONAL BUREAU OF STANDARDS - 1963 - A

12

BUCKLING OF A COMPLETE SPHERICAL SHELL UNDER UNIFORM EXTERNAL PRESSURE

by

Harry E. Rauch, Neal H. Jacobs, and Jonathan L. Marz

Graduate School & University Center
Department of Mathematics
33 West 42 Street
New York, N.Y. 10036

AIR FORCE OFFICE OF SCIENTIFIC RESEARCH (AFSC)
NOTICE OF TRANSMITTAL TO DDC
This technical report has been reviewed and is approved for public release IAW AFR 190-12 (7b).
Distribution is unlimited.
A. D. BLOSE
Technical Information Officer

UNCLASSIFIED

SECURITY CLASSIFICATION OF THIS PAGE (When Data Entered)

(19) REPORT DOCUMENTATION PAGE

READ INSTRUCTIONS BEFORE COMPLETING FORM

(18) 1. REPORT NUMBER: AFOSR - TR - 76 - 1219

2. GOVT ACCESSION NO.

3. RECIPIENT'S CATALOG NUMBER

(6) 4. TITLE (and Subtitle)

BUCKLING OF A COMPLETE SPHERICAL SHELL UNDER UNIFORM EXTERNAL PRESSURE.

5. TYPE OF REPORT & PERIOD COVERED

(9) Interim rept.,

6. PERFORMING ORG. REPORT NUMBER

(10) 7. AUTHOR(s)

Harry E. Rauch, Neal H. Jacobs and Jonathan L. Marz

(15) 8. CONTRACT OR GRANT NUMBER(s)

AF - AFOSR 71-2063-71

9. PERFORMING ORGANIZATION NAME AND ADDRESS

Research Foundation of The City University of NY
Graduate School, Department of Mathematics
33 W 42 Street, New York, N. Y. 10036 409545

10. PROGRAM ELEMENT, PROJECT, TASK AREA & WORK UNIT NUMBERS

61102F (16) 2304/A4 (17) A4

11. CONTROLLING OFFICE NAME AND ADDRESS

Air Force Office of Scientific Research/NM
Bolling AFB, Washington, D.C. 20332

12. REPORT DATE

(11) 1976

13. NUMBER OF PAGES

36

14. MONITORING AGENCY NAME & ADDRESS (if different from Controlling Office)

(12) 44p.

15. SECURITY CLASS. (of this report)

UNCLASSIFIED

15a. DECLASSIFICATION/DOWNGRADING SCHEDULE

16. DISTRIBUTION STATEMENT (of this Report)

Approved for public release; distribution unlimited.

17. DISTRIBUTION STATEMENT (of the abstract entered in Block 20, if different from Report)

18. SUPPLEMENTARY NOTES

19. KEY WORDS (Continue on reverse side if necessary and identify by block number)

non-linear elasticity
buckling of shells
Galerkin method
spectral method
Legendre functions
thin-walled
elasticity
structures
elastic stability

20. ABSTRACT (Continue on reverse side if necessary and identify by block number)

Non-linear axisymmetric blucking of a complete spherical elastic shell under uniform external pressure is treated numerically. Particular attention is given to the lower critical load, which is the theoretical least failure load. Among the new results are the evaluation of this load for thinner shells than those treated in the existing literature; in particular, the values 6.73% and 4.9% of the classical linear buckling loads are obtained for the radius-

→ next page

DD FORM 1 JAN 73 1473 EDITION OF 1 NOV 65 IS OBSOLETE

UNCLASSIFIED 409 545

SECURITY CLASSIFICATION OF THIS PAGE (When Data Entered)

cont. →

20 Abstract

to-thickness ratios 100 and 200 , respectively. The shapes of the buckled shells are computed for the first time in an unexpected hint that there is an asymptotic (ratios-to-thickness ration-independent) buckled shape. Numerical solution is by means of spectral (Galerkin) expansions of up to 60 modes in associated Legendre functions of order one applied to the quadratically non-linear version of E. Reissner's equations.

CAPTIONS FOR FIGURES

Fig. 2 Graph of dimensionless pressure ρ^* versus inward polar deflection (in radii) for a/h = 100, both symmetric and asymmetric branches (see text). Computed with 40 modes through the deflection corresponding to ρ_L^*, then the remainder with 24 modes.

Fig. 3 Analogue of Fig. 2 for a/h = 200. Analogous computations with 60 modes and 40 modes respectively.

Fig. 4 Shape of planar cross-section (through axis of symmetry) of asymmetrically deformed shell for both a/h = 100 and 200 and ρ^* at the respective asymmetric minima. The dashed piece of circle shows the remainder of the undeformed shell; the shapes of the symmetrically deformed shells for $\rho = \rho_L^*$ are not shown because each intersects itself and, hence, is not physically realizable *a priori*.

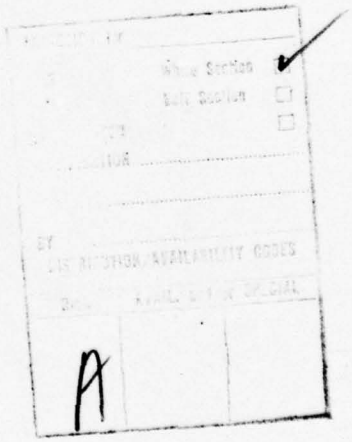

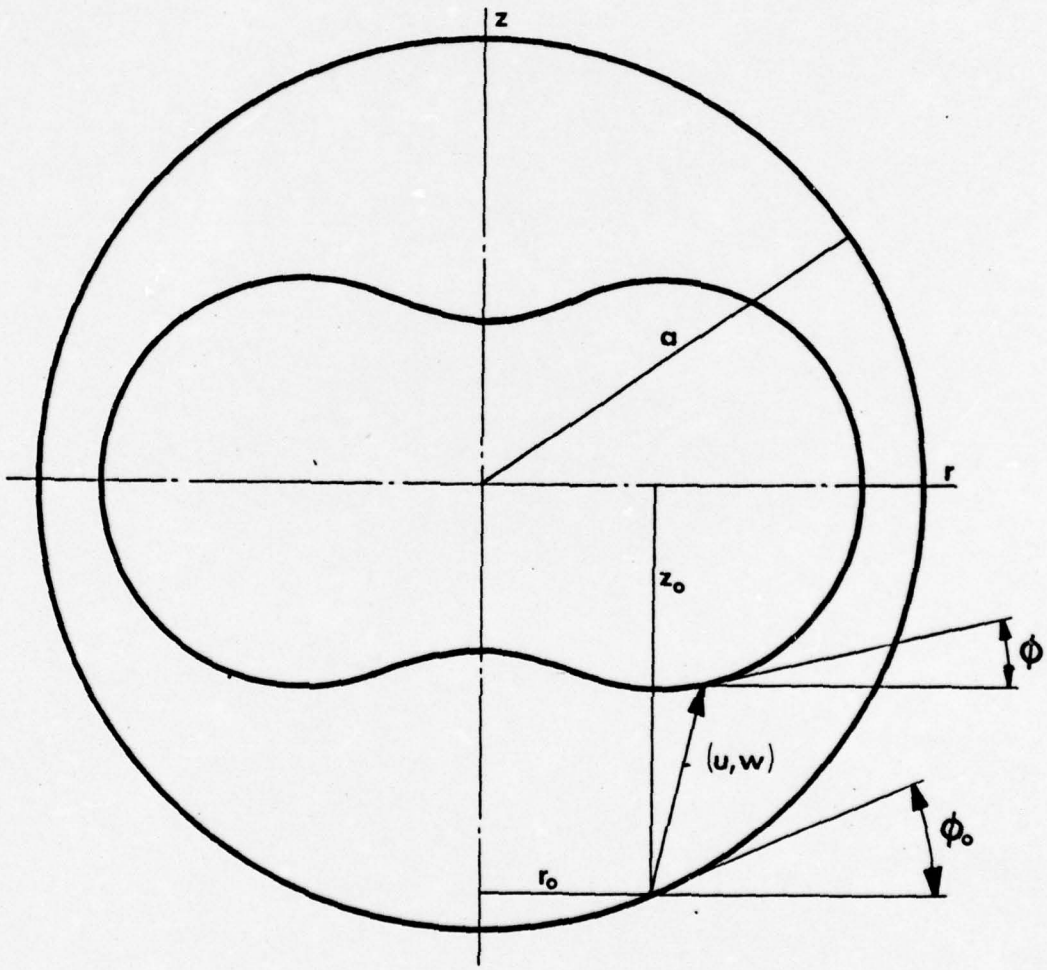
z
a
r
z_o
ϕ
(u,w)
ϕ_o
r_o

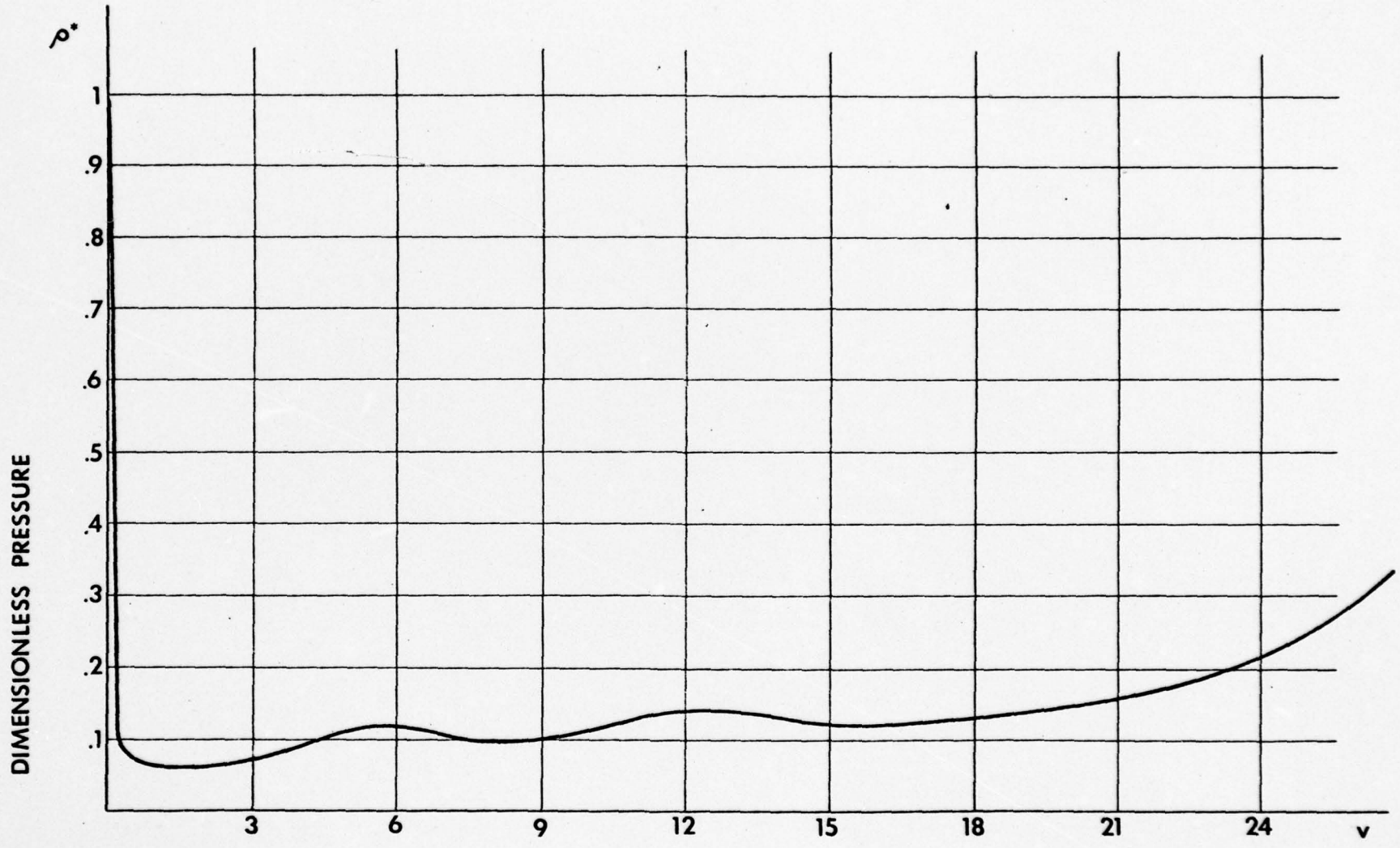
ρ*
1
.9
.8
.7
.6
.5
.4
.3
.2
.1
3
6
9
12
15
18
21
24
v
DIMENSIONLESS PRESSURE
INWARD POLAR DEFLECTION IN RADII

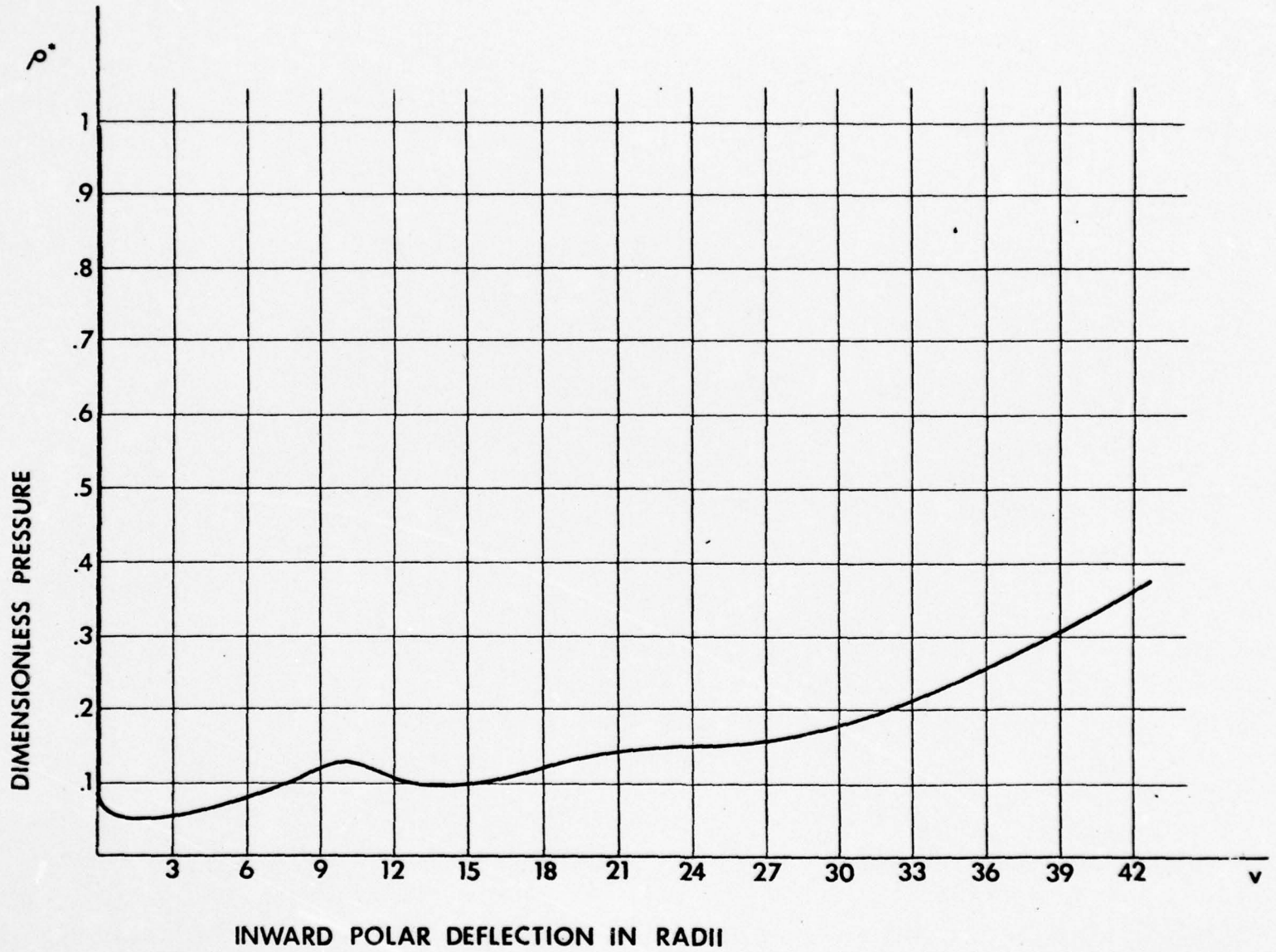
ρ*
1
.9
.8
.7
.6
.5
.4
.3
.2
.1
DIMENSIONLESS PRESSURE
3
6
9
12
15
18
21
24
27
30
33
36
39
42
v
INWARD POLAR DEFLECTION IN RADII

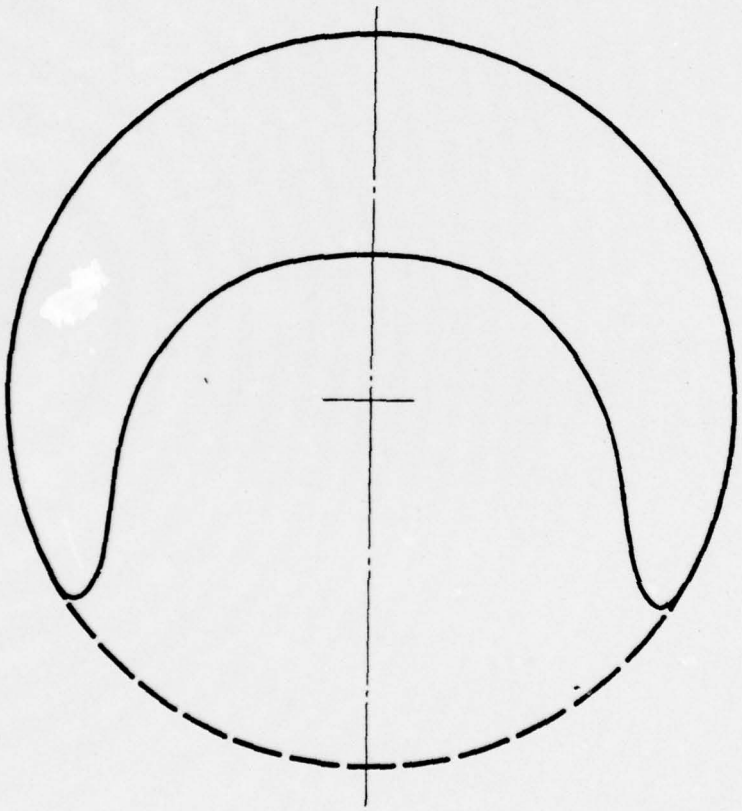

BUCKLING OF A COMPLETE SPHERICAL SHELL UNDER UNIFORM EXTERNAL PRESSURE

by

Harry E. Rauch, Neal H. Jacobs, and Jonathan L. Marz

1. Introduction

A brief history and discussion of the title topic appears in the preliminary sketch of this research, [11], where reference is made to [1], [3], [5], [6], [13], and [14]. The present paper is self-contained.

The immediate goal of the research and the paper is to compute the lower critical pressure of a complete spherical shell for plausible values of radius-thickness ratios. We deal with axisymmetric buckling only here, and this assumption is retained throughout the paper without further mention. It is recalled that the lower critical pressure is the smallest (greatest lower bound)of the pressures for which the initially perfect shell assumes an axisymmetric buckled, i.e., non-spherical shape and thus represents a theoretical absolute least failure load for the shell.under axisymmetric deformation. In view of the marked imperfection sensitivity of the shell ([5], [6], [13], and Section 7 below), the lower critical pressure may, under certain circumstances, be the only reliable theoretical failure load, as was suggested by von Karman and Tsien in their pioneer work. At any rate the low values obtained here, roughly 7% and 5% of the classical linear buckling loads for the radius-thickness ratios 100 and 200, respectively, make the intuitively sensed strength of the complete spherical shell seem illusory. Coupled with related results for the axial compression of circular cylinders ([7], [4]), this indicates the caution necessary in the use of these highly symmetrical thin-walled structures in contrast to flat plates under edge compression, which exhibit postbuckling stability. Indeed, the discovery that certain

"optimized" structures, e.g., flat panels reinforced with stringers, exhibit imperfection-sensitivity when under end compression indicates that it may be necessary more often to perform non-linear lower critical load analyses in addition to the now customary upper critical load, i.e., bifurcation or snap-through analyses.

The basic equations used in the present analysis are the small finite deflection form of E. Reissner's coupled pair of non-linear ordinary differential equations for axisymmetric deformation of axisymmetric shells [12].

The method of solution is a version of the Galerkin or spectral method in which the complete set of functions used is that of the associated Legendre functions of order one. These functions are the formal eigenfunctions of the differential operator appearing in the differential equations so that the linearized system is diagonal. In the opinion of the authors the spectral method has three features to recommend it: (a) it is conceptually simple and relatively straightforward to apply, (b) the resulting Fourier-type analysis of the relevant functions into the various modes is enlightening and relates the non-linear analysis directly to a familiar method of linear analysis, and (c) the method extends directly to certain more complex situations, where partial rather than ordinary differential equations govern.

The progress to be reported here, above and beyond that in [11], is, first, the exhibition of formulas in closed form for the cubic integrals (ℓ,m,n), see Section 3, and the consequent evaluation of them by the program TABLE (see Section 4), and, second, the numerical solution of the coupled quadratic equations obtained from the spectral method by means of the program, SPHERE (see Section 4).

As mentioned in [11], the first-named writer had pursued the present research as far as represented there independently, at which time he became aware of [1], in which the same differential equations (with different interpretations for the dependent variables) are solved by quite a different method, parallel shooting, which is confined in principle to ordinary differential equations. The choice of data presented here is motivated by the desire to give results both of autonomous interest and of sufficiently different character from those in [1] to justify the presentation of the present method as an alternative (see Section 5 for comparison of results). Particular attention is called to Figure 4 and the relevant discussion in Section 5 and the two other "experimental discoveries" there.

Some remarks on a method of incorporating imperfection-sensitivity into the theory given here are given in Section 7.

2. The Basic Equations

The source is Reissner [12, Sections 2-4, 9-11, in particular Eqs. (63)-(69)]. The middle surface of the undeformed spherical shell of radius a and thickness h is represented in cylindrical coordinates (r,z,θ) by $r = r_0 = a \sin \xi$, $z = z_0 = -a \cos \xi$, where ξ is the co-latitude as shown in Fig. 1, where cross sections (say, $\theta = 0$) of the undeformed and deformed shells are shown. Assuming axisymmetric deformation with the z axis as axis of symmetry, one can represent the middle surface of the deformed shell by $r = r_0 + u$, $z = z_0 + w$, where u and w, functions of ξ, are respectively the radial (horizontal) and axial (vertical) components of the displacement vector (u,w). It is important to note that $u < 0$ represents displacement inward toward

the axis of symmetry, while $w > 0$ in the southern hemisphere and $w < 0$ in the northern hemisphere represents displacement inward toward the equatorial plane $z = 0$. The angle between the radial (horizontal) direction and the ray tangent to the meridian of the undeformed middle surface in the direction of increasing ξ at any point with colatitude ξ is denoted by φ_0, and the corresponding angle at the displaced points (coming from those with colatitude ξ) on the deformed middle surface is denoted by φ. (See Fig. 1.)

The first basic dependent variable β is defined by

$$\beta = -(\varphi - \varphi_0) . \tag{1}$$

It is important to observe that in the situation shown in Fig. 1, i.e., an inward directed dimple at the south pole (north pole), one has $\beta > 0$ (< 0).

One defines the stress function ψ by

$$\psi = r_0 H = a(\sin \xi) H , \tag{2}$$

where H is the horizontal (radial) stress resultant at all points on the deformed shell which were originally specified by ξ on the undeformed shell. It is important to observe that near the south pole $\psi < 0$ implies compressive stress, with the same implication for the opposite inequality at the north pole.

If the shell is subjected to a uniform inward normal pressure ρ and is in the membrane state, $\beta \equiv 0$, then one has

$$\psi = -\tfrac{1}{2} \rho a^2 \cos \xi \sin \xi .$$

Now one defines the second basic dependent variable Ψ by

$$\psi = \tfrac{1}{2} \rho a^2 \cos \xi \sin \xi + \Psi \tag{3}$$

so that Ψ describes the deviation of the stress function ψ from the membrane state.

Now, if $D = Eh^3/12(1 - \nu^2)$ is the flexural rigidity, $C = Eh$, where E is Young's modulus, and ν is Poisson's ratio, then the basic differential equations are

$$(4a) \qquad (D/a)[\beta'' + \beta' \cot \xi - (\cot^2\xi + \nu)\beta] = -\psi - \tfrac{1}{2}\rho a^2\beta + \psi\beta \cot \xi ,$$

$$(4b) \qquad \psi'' + \psi' \cot \xi - (\cot^2\xi - \nu)\psi = Ca\beta - \tfrac{1}{2}Ca\beta^2 \cot \xi ,$$

where the prime signifies differentiation with respect to ξ. Equations (4a) and (4b) are deduced from [12, Eqs. (66) and (67)] by setting $P_H = P_V = 0$ and neglecting all terms on the left which do not appear in the classical Reissner-Meissner equations and all those on the right which do not have corresponding terms in the shallow-shell approximations to these equations [12, Eqs. (72) and (73)].

Equations (4a) and(4b) already permit the determination of ρ_L. However, it is desirable to be able to compute the buckled shape of the shell, from β and ψ. For that purpose we consider Eqs. (63), (68), and (69) of [12] and obtain after setting $P_H = P_V = 0$, the dimensionless displacements

$$(5a) \qquad \frac{u(\xi)}{a} = -\frac{(1-\nu)}{2}\,\frac{\rho a}{Eh}\sin\xi + \frac{\psi' \sin\xi}{Eha} - \nu\frac{\psi}{Eha}\cos\xi$$

$$+ \frac{\rho a}{Eh}\beta \sin^2\xi \cos\xi - \nu\frac{\psi}{Eha}\beta \sin\xi$$

$$(5b)\qquad \frac{w(\xi)}{a} = -\frac{(1-\nu)}{2}\,\frac{\rho a}{Eh}\int_{\xi_0}^{\xi}\sin\xi\,d\xi - \int_{\xi_0}^{\xi}\left(1-\frac{(1-\nu)}{2}\,\frac{\rho a}{Eh}\right)\beta\cos\xi\,d\xi$$

$$-\nu\int_{\xi_0}^{\xi}\frac{\psi'}{Eha}\sin\xi\,d\xi + \int_{\xi_0}^{\xi}\frac{\psi}{Eha}\cos\xi\,d\xi$$

$$-\nu\int_{\xi_0}^{\xi}\frac{\rho a}{Eh}\beta\sin^2\xi\cos\xi\,d\xi - \tfrac{1}{2}\int_{\xi_0}^{\xi}\beta^2\sin\xi\,d\xi$$

$$+\int_{\xi_0}^{\xi}\frac{\psi}{Eha}\beta\sin\xi\,d\xi - \int_{\xi_0}^{\xi}\frac{\psi}{Eha}\beta\cot\xi\cos\xi\,d\xi$$

$$+\nu\int_{\xi_0}^{\xi}\frac{\psi'}{Eha}\beta\cos\xi\,d\xi + \nu\int_{\xi_0}^{\xi}\frac{\rho a}{Eh}\beta^2\sin\xi\cos^2\xi\,d\xi\,,$$

where $0 < \xi_0 \leq \pi$ is that value of ξ, to be chosen ad libitum, for which the axial displacement vanishes, i.e., $w(\xi_0) = 0$. The first terms on the right of (5a)-(5b), respectively, are the respective components of the membrane contraction with the normalization indicated.

It should be noted that all cubic terms in Reissner's formulas have been deleted so that this is a "quadratic" theory (see Section 7 below for further comment on this point). The modifications of the equations necessary to study imperfections are indicated in Section 7.

3. Method of Solution of the Equations

The key to the solution of (4a)-(4b) and the subsequent evaluation of (5) is the observation that, the common differential operator

(6) $$( )'' + ( )' \cot \xi - ( ) \cot^2 \xi$$

on the left of (4a)-(4b) can be written

$$( )'' + ( )' \cot \xi - ( )(\csc^2 \xi - 1) = L( ) + 1( ),$$

where

$$L(P_n^1(\cos \xi)) = -n(n+1)P_n^1(\cos \xi),$$

$P_n^1(x)$ being the associated Legendre function of order one and degree n [15, Chapter XV, §15.5]. Thus $P_n^1(\cos \xi)$ is an everywhere finite eigenfunction for (6) with eigenvalue $1 - n(n+1)$.

Two facts about the Legendre polynomials $P_n(x)$ and associated Legendre functions of first order should be noted. One has, with $x = \cos \xi$,

(7a) $$P_n^1(x) = (1 - x^2)^{\frac{1}{2}} dP_n(x)/dx ,$$

(7b) $$(d/d\xi)P_n(\cos \xi) = -(\sin \xi)dP_n(\cos \xi)/dx = -P_n^1(\cos \xi),$$

(7c) $$[d^2P_n(\cos \xi)/d\xi^2] + (\cot \xi)(d/d\xi)P_n(\cos \xi) = -n(n+1)P_n(\cos \xi),$$

(7d) $$(1 - x^2)[d^2P_n^1(x)/dx^2] - 2x(d/dx)P_n^1(x) - [1/(1 - x^2)]P_n^1(x) = -n(n+1)P_n^1(x) .$$

For technical reasons, which will become apparent later, it is convenient to introduce $x = \cos \xi$ as independent variable in (4a)-(4b) to obtain [it should be understood that we are writing $\beta(x) = \beta(\cos \xi)$ rather than $\beta(\xi)$, etc.]

(8a) $$\frac{D}{a}\left[(1 - x^2)\frac{d^2\beta}{dx^2} - 2x\frac{d\beta}{dx} - \left(\frac{x^2}{1-x^2} + \nu\right)\beta\right] = -\psi - \frac{\rho a^2}{2}\beta + \frac{x}{(1-x^2)^{\frac{1}{2}}}\psi\beta ,$$

(8b) $$(1 - x^2)\frac{d^2\psi}{dx^2} - 2x\frac{d\psi}{dx} - \left(\frac{x^2}{1-x^2} - \nu\right)\psi = Ca\beta - \frac{Ca}{2}\beta^2\frac{x}{(1-x^2)^{\frac{1}{2}}} ,$$

since (6) becomes

(9) $$(1 - x^2)(d^2/dx^2)(\ ) - 2x(d/dx)(\ ) - [x^2/(1 - x^2)](\ ).$$

Since $P_n^1(x)$, $n = 1,\ldots,$ form a complete orthogonal set on $(-1,1)$, it seems reasonable to use them to find approximate solutions of (8a)-(8b) for prescribed ρ by the spectral method. We set

(10a) $$\beta = \sum_{n=1}^{s} A_n P_n^1(x)$$

(10b) $$\psi = \sum_{n=1}^{s} B_n P_n^1(x)$$

for fixed s, substitute in (8a)-(8b), expand the right sides out in $P_n^1(x)$, $n = 1,\ldots,$ retaining only the first s terms, and then compare sides.

As a first trivial but vital application of the method we determine the classical linear buckling load ρ_{crit}. Set $\beta = AP_n^1$ and $\psi = BP_n^1$ in the equations obtained from (8a)-(8b) by ignoring nonlinear terms, and obtain

$$(D/a)[1 - n(n+1) - \nu] = -B - \tfrac{1}{2}\rho a^2 A, \quad [1 - n(n+1) + \nu]B = CaA .$$

On eliminating B and assuming $A \neq 0$, one obtains

(11) $$\rho = \frac{2E(h/a)^3}{12(1-\nu^2)}[n(n+1) - 1 + \nu] + \frac{2Eh}{a}\ \frac{1}{n(n+1) - 1 - \nu} .$$

Differentiating (11) with respect to n and equating the result to zero give

(12) $$n(n+1) - 1 - \nu = 2[3(1 - \nu^2)]^{\frac{1}{2}}(a/h) .$$

Substituting in (11) yields

(13) $$\rho_{crit} = \frac{2E}{[3(1-\nu^2)]^{\frac{1}{2}}}\left(\frac{h}{a}\right)^2\left(1 + \frac{\nu}{2[3(1-\nu^2)]^{\frac{1}{2}}}\ \frac{h}{a}\right)$$

$$= \frac{2E}{[3(1-\nu^2)]^{\frac{1}{2}}}\left(\frac{h}{a}\right)^2 L\left(\frac{h}{a}\right),$$

where $L(h/a)$ is the parenthesis.

Returning to (10), we define

$$(14a) \qquad (\ell,m,n) = \int_{-1}^{1} \frac{x}{(1-x^2)^{\frac{1}{2}}} P_\ell^1(x)P_m^1(x)P_n^1(x)dx$$

$$= \int_{-1}^{1} x(1-x^2)\frac{dP_\ell}{dx}\frac{dP_m}{dx}\frac{dP_n}{dx}\,dx\,,$$

$$(14b) \qquad j_n = \int_{-1}^{1} (P_n^1)^2\,dx = \frac{2n(n+1)}{2n+1}$$

and carry out the spectral method, first, by substituting (10) in (8b) and comparing sides to obtain

$$(A) \qquad B_n = -\{Ca/[n(n+1)-1-\nu]\}A_n + \{Ca/2[n(n+1)-1-\nu]\}\sum_{\ell,m=1}^{s}[(\ell,m,n)/j_n]A_\ell A_m,$$

$n = 1,\ldots,s$, and then by substituting (10) in (8a) to obtain

$$(B) \qquad (\tfrac{1}{2}\rho a^2 - (D/a)[n(n+1) - 1+\nu])A_n = -B_n + \sum_{\ell,m=1}^{s}[(\ell,m,n)/j_n]A_\ell B_m,$$

$$n = 1,\ldots,s\,.$$

We introduce the dimensionless variables

$$(15) \qquad B_n^* = B_n/\rho_{crit}\,a^2\,,$$

$$\rho^* = \rho/\rho_{crit} = \rho a^2/\rho_{crit}\,a^2\,.$$

Dividing equations (A) and (B) by $\rho_{crit}a^2$, multiplying (B) by two, and using (15) give

$$(A') \qquad B_n^* = -\frac{[3(1-\nu^2)]^{\frac{1}{2}}}{2L(h/a)[n(n+1)-1-\nu]}\frac{a}{h}A_n + \frac{[3(1-\nu^2)]^{\frac{1}{2}}}{4L(h/a)[n(n+1)-1-\nu]}\frac{a}{h}\sum_{\ell,m=1}^{s}\left[\frac{(\ell,m,n)}{j_n}\right]A_\ell A_m\,,$$

$$(B') \qquad \left\{\rho^* - \frac{h}{a}\frac{n(n+1)-1+\nu}{4[3(1-\nu^2)]^{\frac{1}{2}}L(h/a)}\right\}A_n + 2B_n^* - 2\sum_{\ell,m=1}^{s}\left[\frac{(\ell,m,n)}{j_n}\right]A_\ell B_m^* = 0\,,\quad n = 1,\ldots,s.$$

To compute the shape of the shell corresponding to any solution $\rho^*, A_1,\ldots,A_s, B_1^*,\ldots,B_s^*$ of (A') and (B') we represent the middle surface in dimensionless form as

$$\frac{r}{a} = \frac{r_0}{a} + \frac{u}{a} = \sin\xi + \frac{u}{a} \tag{16}$$

$$\frac{z}{a} = \frac{z_0}{a} + \frac{w}{a} = -\cos\xi + \frac{w}{a}$$

and write in Eqs. (5a) and (5b),

$$\frac{\rho a}{Eh} = \left(\frac{h}{a}\right)\frac{2L(h/a)\rho^*}{\sqrt{3(1-\nu^2)}} \tag{17}$$

$$\frac{\psi}{Eha} = \left(\frac{h}{a}\right)\frac{2L(h/a)\psi^*}{\sqrt{3(1-\nu^2)}} \quad .$$

With the last definition one has

$$\psi^* = \sum_{n=1}^{s} B_n^* P_n^1(\cos\xi) \ ,$$

and if one substitutes this and the truncated series for β in (16) and (17) then numerical integration using the trapezoidal rule yields the shape. The shape computation was effected by a simple auxiliary FORTRAN program. The value of ξ_0 was taken to be π, i.e., the <u>north pole</u> was taken to be fixed. The advantage of such a normalization will be apparent in a moment.

In the program SPHERE (see Section 4) used to solve (A') and (B') it was necessary to incorporate a subroutine which for each solution $\rho^*, A_1,\ldots$ computes some convenient deflection parameter. At first glance (and in [11]) it seems reasonable to use the south polar deflection under the assumption that the <u>equator</u> is fixed ($\xi_0 = \pi/2$). In hindsight, if the above mentioned auxiliary program had been used as the subroutine, as is possible, then the fixed equator hypothesis would have been as

easy to implement. However, the original polar deflection subroutine uses the coefficients $A_1,\ldots,A_s$; $B_1^*,\ldots,B_s^*$ directly, and there as will be seen in Section 6, the simplification brought about by setting $\xi_0 = \pi$ is enormous. We then decided that <u>half</u> the resulting deflection is the useful parameter for the symmetric deformations (see Section 5). Since the resulting formulas are in SPHERE and may be of independent interest, we reproduce them here.

We define

$$(18)\qquad \Delta(m,n) = \Delta(n,m) = \begin{cases} 0 & m \neq n \\ \dfrac{2}{2m+1} & m = n \end{cases},$$

$$p(n) = \begin{cases} 0 & n \equiv 0 \ (2) \\ 1 & n \equiv 1 \ (2) \end{cases}$$

$$q = \begin{cases} 1 & \text{asymmetric deformation} \\ 2 & \text{symmetric deformation.} \end{cases}$$

$$K = \left(\frac{h}{a}\right) \frac{2L(h/a)}{\sqrt{3(1-\nu^2)}} .$$

Then the polar deflection parameter v is given by

$$(19)\quad qv = \frac{w(0)}{a} = (1-\nu)K\rho^* + \left(1-\frac{(1-\nu)}{2}K\rho^*\right)\sum_{n=1}^{s}(1-(-1)^{n+1})A_n$$

$$+ (1+\nu)K\sum_{n=1}^{s}(1-(-1)^{n+1})B_n^* + \frac{4\nu}{5}K\rho^*A_2 + \sum_{n=1}^{s}\frac{n(n+1)}{2n+1}A_n^2$$

$$- K\sum_{n=1}^{s}\frac{2n(n+1)}{2n+1}A_nB_n^* + (1+\nu)K\left[\sum_{n=1}^{s}\frac{2n^2}{2n+1}A_nB_n^*\right.$$

$$+ \sum_{n=1}^{s} mB_m^* \sum_{n=1}^{s} A_n \sum_{j=1}^{(n-1+p(n-1))/2} (4j - 2p(n-1)-1)\Delta(m,2j - 2p(n-1)-1)$$

$$+ \sum_{n=1}^{s} nA_n \sum_{m=1}^{s} B_m^* \sum_{i=1}^{(m-1+p(m-1))/2} (4i - 2p(m-1)-1)\Delta(n,2i - 2p(m-1)-1)$$

$$+ \sum_{m=1}^{s} B_m^* \sum_{n=1}^{s} A_n \sum_{i=1}^{(m-1+p(m-1))/2} \sum_{j=1}^{(n-1+p(n-1))/2} (4i - 2p(m-1))(4j-1-p(n-1))$$

$$\times\ \Delta(2i - 2p(m-1) - 1\ ,\ 2j - 2p(n-1) - 1)\Big]$$

$$- \nu K\Big[\sum_{m=1}^{s} \frac{2m^2(m+1)}{2m+1} A_m B_m^* + \sum_{m=1}^{s} m(m+1) B_m^* \sum_{n=1}^{s} A_n$$

$$\times \sum_{i=1}^{(n-1+p(n-1))/2} (4i - 2p(n-1) - 1)\,\Delta(m, 2i - p(n-1) - 1)\Big]$$

$$- 2\nu K\rho^*\Big[\sum_{n=1}^{s-2} \frac{2n(n+1)(n+2)(n+3)}{(2n+1)(2n+5)(2n+3)} A_n A_{n+2}$$

$$- \sum_{n=1}^{s} \frac{2n^2(n+1)^2}{(2n+1)(2n-1)(2n+3)} A_n^2 + \sum_{m=1}^{s} \frac{m(m+1)}{2m+1} A_m \sum_{n=1}^{s} A_n$$

$$\times \sum_{i=1}^{(n+p(n))/2} (4i - 2p(n) - 1)\,\Delta(m-1, 2i - p(n) - 1)$$

$$- \sum_{m=1}^{s} \frac{m(m+1)}{2m+1} A_m \sum_{n=1}^{s} A_n \sum_{i=1}^{(n+p(n))/2} (4i - 2p(n) - 1)\,\Delta(m+1, 2i - p(n) - 1)\Big] \ .$$

This formula will be established in Section 6. In practice only the linear and the first non-linear terms make significant contributions.

4. Numerical Methods

For given a/h, ν, and s numerical solution of the equations (A') and (B') was performed by means of the program SPHERE, written for this purpose but adaptable to other sets of non-linear equation. SPHERE is modeled on the algorithm proposed by E. Polak [10]. The essence of the algorithm is a combination of the secant method with the method of local variations. We found it to be very powerful.

Already in our first version of SPHERE, a PL/I double precision program, we omitted certain convergence accelerating features at the end of Polak's algorithm. It should be pointed out that there was little hope that Polak's hypothesis on invertibility of the Jacobian would be verified

in our case and, thus, little hope of global convergence. Indeed, in continuation of solutions near the first relative minima of the pressure-deflection graphs we often encountered suggestions of possible zero Jacobians in the form of loss of significance messages from the linear inversion subroutine. Correspondingly, we had little success in using SPHERE to find many-mode solutions starting from wild guesses. Accordingly the necessity for good starting and continuation procedures manifested itself early. We shall describe some below.

Equations (A') and (B') were cast in the functional form $G(A) = 0$, where $G(A)$ is a vector with s components, by putting all terms on the left side in each equation of (B') and then, for each attempted solution vector $A_1,\ldots,A_s$, substituting the vector $B_1^*,\ldots,B_s^*$ computed from (A') into (B'). As a criterion for a "solution" we used $\|G(A)\| \leq \epsilon$, where the norm is the usual vector norm, and ϵ was a predetermined small number, usually 10^{-5}.

The coefficients (ℓ,m,n) required in $G(A) = 0$ for a given s were computed by a program TABLE on the basis of equation (27) in Section 6 and put on a disk which was read into core when SPHERE was run. Because of the large size of the three-way array (ℓ,m,n) for realistic s - despite the symmetry and vanishing properties of Section 6, which reduce 64,000 to 3270 for $s = 40$, for example - and the initial demand for double precision a linearization routine for both TABLE and SPHERE was written (by James Korenthal). However, it developed that single precision was quite adequate and that the linearization was quite time consuming so that the (ℓ,m,n) could be read in directly with tolerable core requirements and very substantial savings. Ultimately a still simpler and faster FORTRAN version of SPHERE was prepared. Copies of all programs

described in this paper are available by request from the authors.

All discussion of accuracy and starting and continuation procedures hinges on the notions of critical mode and supercritical mode. Here, a mode is one the A's, the n-th mode is A_n, and n is the index of that mode. Then a mode is critical for a given value of a/h if its index minimizes the expression (11) for ρ obtained from the assumption of linear buckling or, equivalently, the expression for ρ^* obtained by dividing (11) by (13), where a/h is the given value. The mode whose index differs from the minimizing index by one and whose associated value of ρ^* is the next lowest is also called critical. Thus to each value of a/h is associated uniquely a pair of critical modes whose indices are consecutive integers, in particular, one odd and one even. For the two values of a/h, 100 and 200, handled explicitly in this paper one has, for $a/h = 100$, the values $\rho^* = 1.019939, 1,003290, 1.000465, 1.009291$ associated with the indices 16, 17, 18, 19, respectively, all other indices giving higher values, so that the seventeenth and eighteenth modes are critical with the even mode having lowest ρ^*. Similarly for $a/h = 200$ one has $1.004888, 1.000174, 1.001709$ corresponding to 24, 25, 26, respectively, so that modes 25 and 26 are critical with the odd mode having lowest ρ^*. A supercritical mode for given a/h is one whose index is greater than those of the critical modes for that a/h.

The critical modes play a role, first, in starting procedures. The basic starting strategy to find a solution of $G(A) = 0$ for given ρ^* and a/h is to solve the smallest number of equations possible, i.e., use the smallest number of modes possible, and then extend this solution to one with more modes by using its entries as the initial entries of a guess for a higher number of modes, with the remainder of the entries being zeros. We call this strategy extending a solution by zeros. It

is hampered, however, by the peculiar fact, discovered in the course of the numerical work, that it does not work unless the number of modes or, equivalently, the index of the last (highest index) mode of the solution to be extended is greater than the indices of the critical modes for that a/h. More precisely, only solutions already containing supercritical modes can be extended by zeros to obtain solutions with (even more) supercritical modes.

"Subcritical" solutions can often be extended by zeros to "longer subcritical" solutions, but these cannot be extended further and represent spurious approximations to solutions, analogous to the extraneous solutions to the difference equations sometimes obtained when applying finite-difference methods to differential equations.

Accordingly it is necessary to start by assuming small, quite unphysical, values of a/h such as .5 for which A_2 is supercritical. For fixed ρ^* (for example, a little less than 1, if one is starting a pressure-deflection graph of the postbuckling regime) one solves for A_1, A_2 by starting with any reasonable initial vector, say, (1,0) - an even more surefire technique is given below. The resulting solution is then extended by zeros with a sufficiently large number of terms so that the last index is supercritical for a higher value of a/h, say, 5. The resulting solution is then continued by letting a/h vary from the starting value to the new value. The new solution is then extended by zeros until supercritical for a higher value of a/h, and so on until a solution at the desired a/h is obtained. This is called zig-zagging. It proved to be more efficient to zig-zag in reasonably small increments of a/h rather than to attempt to, say, extend the initial solution to be supercritical for the final value of a/h and then to continue to that value. Also, it was found to be much easier to extend solutions by

zeros or continue solutions in the parameter a/h for ρ^* near 1 and small deflections rather than for ρ^* near ρ_L^* and the corresponding large deflections.

A pressure-deflection graph is not monotone in principle, and the approximations to it obtained by truncating the expansions at too small an index are often even more oscillatory. Hence, the vital feature of continuation by changing one of the A's, typically A_1 or A_2 for asymmetric or symmetric solutions (see Section 5), respectively, and solving for ρ^* as one of the unknowns was built into the program. Once this was done it was found that it was much more efficient to use this method of continuation even on monotone branches so that solution with ρ^* fixed and continuation by varying ρ^* were used ultimately only in the starting procedure mentioned above. It was found that, in general, although not always, the polar deflection is a monotone increasing function of A_1 or A_2.

For very large values (say, > 15 radii) of the polar deflection and correspondingly large A's it is necessary to relax the demand on the norm of the residuals by several orders of magnitude in order to continue computing the graph efficiently since the residuals are extremely sensitive to small changes in the A's when the first few of the latter are large, as one sees by inspecting (A') and (B'). However, any one solution can be refined and the effect on the graph is visually imperceptible. It should be noted that if one distinguishes <u>symmetric</u> from <u>asymmetric</u> solutions to (4) (see Section 5) then the associated truncated expansions can be identified easily. In fact, as noted there, the coefficients A_n and B_n with odd n vanish for a symmetric solution. This reduces the actual number of variables for even s to $s/2$. SPHERE is programmed to take advantage of this by handling only variables with even indices

upon receipt of the proper input, effecting a very substantial saving in computing time.

Finally we outline a foolproof procedure for solving $G(\Lambda) = 0$ when $s = 2$. We note that by properties of the (ℓ,m,n) obtained in Section 6, $(1,1,1) = (2,2,1) = (2,1,2) = (1,2,2) = 0$ and $(2,1,1) = (1,2,1) = (1,1,2)$. For $s = 2$ (A') and (B') become

$$B_1^* = \frac{\sqrt{3(1-\nu^2)}}{2L(h/a)(1-\nu)}\left(\frac{a}{h}\right)\left(-A_1 + \frac{3}{4}(2,1,1)A_2A_1\right)$$

$$B_2^* = \frac{\sqrt{3(1-\nu^2)}}{2L(h/a)(5-\nu)}\left(\frac{a}{h}\right)\left(-A_2 + \frac{5}{24}(1,1,2)A_1^2 + \frac{5}{24}(2,2,2)A_2^2\right)$$

$$\left(\rho^* - \left(\frac{h}{a}\right)\frac{(1+\nu)}{4\sqrt{3(1-\nu^2)}L(h/a)}\right)A_1 = -2B_1^* + \frac{3}{2}(1,2,1)A_1B_2^* + \frac{3}{2}(2,1,1)A_2B_1^*$$

$$\left(\rho^* - \left(\frac{h}{a}\right)\frac{(1+\nu)}{4\sqrt{3(1-\nu^2)}L(h/a)}\right)A_2 = -2B_2^* + \frac{5}{6}(1,1,2)A_1B_1^* + \frac{5}{6}(2,2,2)A_2B_2^* .$$

If one sets $A_1 = 0$, $B_1^* = 0$ so that one is seeking a symmetric solution, then one sees that the first and third equations are identically satisfied. One could then substitute the second in the fourth to obtain an explicit cubic for A_2 which could be solved numerically, but that is not necessary if one is using SPHERE since the use of initial guess vectors with the first component zero is equivalent to solving that cubic by a secant-local-variation method. If, however, one desires an asymmetric solution, so that $A_1 \neq 0$, then one finds that substitution of the first two equations in the third leads to a cubic equation in A_1 and A_2 every term of which contains A_1 to the first or third power. Cancellation of A_1 leads to a quadratic which can be solved explicitly for A_1^2 as follows.

$$A_1^2 = \left[\frac{(2,2,2)}{(1,1,2)} + \frac{18(5-\nu)}{5(1-\nu)}\right]A_2^2 + \frac{96}{5}\frac{1}{(1,1,2)}\frac{(3-\nu)}{(1-\nu)}A_2$$
$$+ \frac{32}{5}\frac{(5-\nu)}{(1-\nu)}\frac{1}{(1,1,2)^2}\left[\frac{L(h/a)(1-\nu)}{\sqrt{3(1-\nu^2)}}\left(\frac{h}{a}\right)\rho^* - 1 - \frac{1}{12}\left(\frac{h}{a}\right)^2\right].$$

Again this equation could be substituted along with the first and second equations into the fourth equation to obtain an explicit cubic in A_2 whose solution together with this equation would solve $G(A) = 0$ for $s = 2$. But, again, it is more suitable, if one has guessed A_2, to calculate A_1 from the preceding equation and use the resulting A_1, A_2 as input for the program.

It should be mentioned that the discussion of imperfection-sensitivity at the end of Section 7 suggests another starting procedure. What makes starting so difficult for (A') and (B') is that they are homogeneous so that they possess a solution whose entries are all zero. By inserting a non-zero imperfection parameter ϵ_n in the equations at the end of Section 7 one obtains inhomogeneous equations of which non-trivial solutions which continue the trivial solution for $\rho^* = 0$ are easily found for small ρ^*. Continuation to the relative maximum (or maxima) and then to the downward sloping part of the graph followed by continuation in ϵ_n as $\epsilon_n \to 0$ would yield non-trivial solutions of the equations for the perfect shell which could then be continued for smaller or larger deflection.

5. Numerical Results

As a preliminary we note that replacing ξ by $\pi - \xi$ in (4) while replacing β, ψ by $-\beta, -\psi$, respectively, shows that if $\beta(\xi)$, $\psi(\xi)$ are a solution then $-\beta(\pi-\xi)$, $-\psi(\pi-\xi)$ are, too. Equivalently, (with the same abuse of functional notation remarked on in Section 2)

$-\beta(-x)$, $-\psi(-x)$ are also a solution of (8). From the remarks at the beginning of Section 2 it is clear that this means the physically obvious fact that if one has a buckled shell then the mirror image in the equatorial plane of the unbuckled shell is also a buckled shell. In particular, a solution β, ψ for which $\beta(\xi) = -\beta(\pi-\xi)$, $\psi(\xi) = -\psi(\pi-\xi)$ or, equivalently, $\beta(x) = -\beta(-x)$, $\psi(x) = -\psi(-x)$ will be called <u>symmetric</u> because it manifestly represents a buckled shape symmetric with respect to the equatorial plane. By the preceding remarks the <u>asymmetric</u> solutions come in pairs, one being the mirror image (in the equatorial plane) of the other. In terms of the truncated expansions of β and ψ one observes that $P_n^1(x) = (1-x^2)^{\frac{1}{2}} dP_n/dx$ and the fact that $P_n(x)$ is even or odd according as n is, together with $\beta(x) = -\beta(-x)$, $\psi(x) = -\psi(-x)$ imply $A_n = B_n^* = 0$ for odd n, that is, a solution is symmetric if and only if terms with even indices only appear in the expansions. For this reason symmetric solutions are referred to as <u>even</u> in our programs although, in fact, they are <u>odd</u> as functions of x. Similar reasoning shows that one of the paired, mirror-image, asymmetric solutions differs precisely from the other in the signs of the terms of odd index. The presence of terms with odd indices in the expansions of asymmetric solutions led us to call them <u>odd-even</u> in the programs although they are neither odd nor even.

For all the values of a/h used in our work we found for any even supercritical s three solution branches of $G(A) = 0$ issuing from the vicinity of $\rho^* = 1$, $A_1 = \ldots = A_s = 0$, i.e., the (unbuckled) membrane solution at the classical linear buckling pressure. By a solution branch we mean a one-parameter family of values of ρ^* and associated

non-trivial vectors A each of which satisfies $G(A) = 0$ for the associated value of ρ^*. The parameter is either ρ^* itself or one of the A's, usually A_1 or A_2. One of the branches consists of symmetric solutions and issues from the point for which ρ^* is the value associated with the critical mode of even index for the given a/h, and the other two issue from the corresponding point for the critical mode of odd index, any one of the two representing the mirror images of the solutions of the other. When the value of ρ^* and the value of the polar deflection, which, we recall, is the right side of (18) for asymmetric solutions and half that for symmetric ones, are plotted as ordinate and abscissa, respectively, one obtains <u>two</u> pressure deflection graphs, <u>one</u> for the symmetric solution branch and <u>one</u> for the two mirror image asymmetric solution branches since, as one verifies from (5b), the pola- deflection is the <u>same</u> for mirror images. We ignore the prebuckling linear membrane pieces of the graphs since they play no role in determining ρ_L^*. However, if imperfection-sensitivity were studied in the way sketched in Section 7, then the corresponding parts of the graphs would be quite important and would require much larger scales than those of Figures 2 and 3 here.

We take the lesser of the absolute minima of the two graphs in question for given a/h to be ρ_L^*. Now for $a/h = 100, 200$, the two cases handled <u>in extenso</u>, the two graphs, symmetric and asymmetric solutions, in each case are, most remarkably, virtually coincident and certainly so when graphed on any reasonable scale. For that reason Figure 2 actually is two graphs, and the same is true of Figure 3. The second interesting fact is that for both 100 and 200 the asymmetric minimum proved greater than the symmetric minimum but only by at most one digit in the last

significant figure retained. In [1] for $a/h = 9.13$ (their Figure 1b) it is also true that the symmetric minimum is less than the asymmetric minimum. On the hypothesis that this is always true for $9.13 \leq a/h \leq 200$ we have included two other sets of data in Table 1, a table of lower critical pressures. One is a run for $a/h = 21.4$ we made for symmetric solutions only and the other for $a/h = 91.3$ is taken from Figure 9 of [1] by graphical estimation. Other data included in Table 1 for the sake of comparison are the values of k and P_L, the parameters used in [1], corresponding to our a/h and ρ_L^*, respectively, as well as the deflection parameter A of [1] for the relevant solutions and our polar deflection parameter v for our solutions and those of [1] where graphical estimation permitted us to determine it. A is a root mean square deflection, which we did not compute for our solutions.

We call attention to another unanticipated result of our computations. Figure 4 is the shape of the asymmetrically deformed shell for $\rho = \rho_L^*$ at $a/h = 100$, but it is also the shape of the corresponding shell for $a/h = 200$, within the tolerance of the graphical realization. There is a hint here of an asymptotic shape as $a/h \to \infty$. If one regards the shell as an inextensible membrane then a classical theorem of differential geometry in the large implies that the shell is rigid, i.e., admits no (differentiable) bending. The only possible deflected shape is obtained in the obvious way by violating differentiability and sawing off a cap and reversing it. Now a careful inspection of Figure 4 discloses that the indentation resembles a piece of sphere of radius a subject to increasingly strong bending. But in the absence of elasticity theory there is no a priori reason to select one size of cap over another, whereas Figure 4 shows that the non-linear elasticity theory embodied in Reissner's equations predicts a definite size, a central angle of a

little less than 120° for $a/h = 100$, 200 and possibly asymptotically.

Two final points of discussion: accuracy and physical significance. The figures in Table 1 for $a/h = 100$ and 200 are accurate at least to the number of significant figures shown. This was determined by increasing the number of modes until the figures stabilized. The results shown used 40 modes for $a/h = 100$ and 60 for $a/h = 200$. The last probably approaches the limit of the present codes within practicable computer times. More modes and greater a/h require improved codes (see Section 7). As a sample of our results Table 2 shows $A_1,\ldots,A_{40}$; $B_1^*,\ldots,B_{40}^*$ (rounded to four figures to save space) for $a/h = 100$, $\rho^* = .0674$, which is the asymmetric minimum.

As far as physical significance is concerned the likelihood or lack of it of realizing deflections of the magnitude shown in Figure 4 is discussed in Section 7. However, the physical usefulness of the values of ρ_L^* in Table 1 for the <u>thin</u> shells ($a/h \geq 91.3$) should not be dismissed lightly. Discussions of imperfection-sensitivity indicate that the snap-through load can be degraded substantially toward ρ_L^*.

TABLE 1

LOWER CRITICAL PRESSURES

a/h	k [1]	ρ_L^*	P_L [1]	v	A [1]
9.13**	10^{-3}	15.7 %	.0105	3.4 §	2.5 §
21.4	1.82×10^{-4}	12.4 %†	3.52×10^{-3} †	3.91 †	-
91.3**	10^{-5}	7.2 %†§	4.8×10^{-4}†§	-	1.2 §
100	8.3×10^{-6}	6.73 %	4.08×10^{-4}	1.41	-
200	2.08×10^{-6}	4.9 %	1.5×10^{-4}	1.4	-

**Results from [1] .

†Computed from symmetric solutions only.

§Estimated from graphs in [1].

TABLE 2

EXPANSION COEFFICIENTS, a/h = 100, v = 1.41, $\rho^* = .0674$, $\rho_L^* = .0673$

A's (read by rows; 3.063 - 1 = 3.063×10^{-1}, etc.).

3.063-1	3.706-1	2.982-1	1.400-1	-1.858-2
-1.054-1	-9.791-2	-2.906-2	4.070-2	6.475-2
3.749-2	-1.000-3	-3.911-2	-3.306-2	-4.589-3
2.011-2	2.398-2	9.561-3	-7.882-3	-1.494-2
-9.381-3	1.319-3	8.077-3	7.192-3	1.462-3
-3.669-3	-4.740-3	-2.156-3	1.208-3	2.753-3
1.912-3	-3.514-5	-1.396-3	-1.380-3	-3.949-4
5.859-4	8.719-4	4.585-4	-1.693-4	-5.175-4

B's

-1.462-2	-1.201-2	-6.366-4	1.110-2	1.474-2
8.111-3	-3.290-3	-1.081-2	-9.419-3	-1.305-3
6.499-3	8.153-3	3.446-3	-2.888-3	-5.743-3
-3.724-3	5.447-4	3.353-3	3.002-3	5.751-4
-1.605-3	-2.030-3	-8.863-4	5.649-4	1.200-3
8.022-4	-4.930-5	-6.201-4	-5.882-4	-1.505-4
2.667-4	3.756-4	1.886-4	-7.707-5	-2.125-4
-1.601-4	-1.033-5	1.054-4	1.173-4	4.803-5

6. Legendre functions and the coefficients (ℓ,m,n)

We need the recursion formulas [15, §15. 21]

$$(20)\qquad xdP_n/dx = nP_n + dP_{n-1}/dx$$

$$(21)\qquad (1-x^2)dP_n/dx = nP_{n-1} - nxP_n$$

$$(22)\qquad xP_n = [(n+1)/(2n+1)]P_n + [n/(2n+1)]P_{n-1}$$

$$(23)\qquad dP_n/dx = dP_{n-2}/dx + (2n-1)P_{n-1} .$$

From (20) and (21) we deduce

$$(24)\qquad (1-x^2)dP_n/dx = [n(n+1)/(2n+1)](P_{n-1} - P_{n+1}) .$$

From (22) by induction we deduce

$$(25)\qquad dP_n/dx = \sum_{j=1}^{(n+p(n))/2} (4j-1-2p(n))P_{2j-1-p(n)}$$

Finally from (20) and (25) we deduce

$$(26)\quad xdP_n/dx = nP_n + \sum_{j=1}^{((n-1)+p(n-1))/2} (4j-1-2p(n-1))P_{2j-1-p(n-1)}$$

$$= nP_n + \sum_{j=1}^{(n-p(n))/2} (4j-3+2p(n))P_{2j-2+p(n)} ,$$

since $p(n-1)=1-p(n)$.

Now apply (25) with $n = \ell$, (24) with $n = m$, and (26) to obtain

$$(27)\qquad (\ell,m,n) = \int_{-1}^{1} x(1-x^2)\,\frac{dP_\ell}{dx}\,\frac{dP_m}{dx}\,\frac{dP_n}{dx}\,dx$$

$$= \frac{m(m+1)}{2m+1} \sum_{i=1}^{(\ell+p(\ell))/2} (4i-1-2p(\ell))\{n[P(2i-1-p(\ell),m-1,n)$$

$$- P(2i-1-p(\ell),m+1,n)] + \sum_{j=1}^{(n-p(n))/2} (4j-3+2p(n))$$

$$\times [P(2i-1-p(\ell),m-1,2j-2+p(n)) - P(2i-1-p(\ell),m+1,2j-2+p(n))]\} ,$$

where $$P(\ell,m,n) = \int_{-1}^{1} P_\ell P_m P_n \, dx \ .$$

Now according to a result of Ferrers and Adams [15, p. 331],[13, p.306]

(28) $$\int_{-1}^{1} P_\ell P_m P_n \, dx = \begin{cases} \dfrac{2}{2\epsilon+1} \dfrac{A(\epsilon-\ell)A(\epsilon-m)A(\epsilon-n)}{A(\epsilon)} \\ 0 \quad \text{if } \ell+m+n \text{ is odd or if sum of two indices is less than the third,} \end{cases}$$

where $\epsilon = \frac{1}{2}(\ell+m+n)$, $A(k) = 1\cdot 3 \cdots (2k-1)/k!$, $k > 0$, $A(0) = 1$. For programming purposes it is better to extend the definition of $A(k)$ by setting $A(k) = 0$, $k < 0$, in which case the two-index sum property becomes a consequence of the top line of (28). It is clear that $P(\ell,m,n)$ is symmetric in ℓ,m,n . It is clear that $P(\ell,m,n) = 0$ if $\ell+m+n$ is odd because the integrand is then an odd function. That $P(\ell,m,n) = 0$ if, say, $\ell > m+n$ follows from the fact that the Legendre polynomial P_ℓ is orthogonal to all polynomials of lower degree, in particular, $P_m P_n$.

It is important that (ℓ,m,n) has the same symmetry and vanishing properties as $P(\ell,m,n)$. The symmetry is obvious from the definition (14a). Again, if $\ell > m+n$ then

$$(\ell,m,n) = \frac{\ell(\ell+1)}{2\ell+1} \int_{-1}^{1} (P_{\ell-1} - P_{\ell+1}) x \frac{dP_m}{dx} \frac{dP_n}{dx} \, dx$$

by (24). But the factor of the integrand outside the parenthesis is a polynomial of degree $m+n-1$, and both $P_{\ell-1}$ and $P_{\ell+1}$ are orthogonal to it since $\ell+1 > \ell-1 > m+n-1$. Finally, the same formula shows that if, say, ℓ is odd and m and n even then $(\ell,m,n) = 0$ since the integrand is odd. The same is true of ℓ,m,n all odd. This exhausts the cases where $\ell+m+n$ is odd for fixed ℓ in the first position. By symmetry, then, $(\ell,m,n) = 0$ for $\ell+m+n$ odd.

We now wish to establish the enumerative formulas

(29) $\frac{1}{48}\left[N^3 + (N-2)^3 + 12(N^2+(N-2)^3) + 20(N+N-2)\right],$

$\frac{1}{24}\left[(N-1)^3 + 12(N-1)^2 + 20(N-1)\right]$

for the number of distinct non-zero (ℓ,m,n) with $\ell,m,n \le N$ with N even or odd, respectively, i.e., in view of the symmetry, the number of non-zero (ℓ,m,n) with $N \ge \ell \ge m \ge n$. We reason as follows. If N is even, then there are $N/2$ (ℓ,m,n), $\ell \ge m \ge n$, of the form $(N,N,2k)$, namely, for $k = 1,\ldots,N/2$; $N/2$ of the form $(N,N-1,2k-1)$, namely, for $k = 1,\ldots,N/2$; $N/2 - 1$ of the form $(N,N-2,2k)$, namely, for $k = 1,\ldots,N/2-1$; $N/2-2$ of the form $(N,N-3,2k-1)$, namely, for $k = 2,\ldots,N/2-1$; etc., down to $1 = N/2 - (N/2-1)$ of the form $(N,N/2,N/2)$ for a total of $N/2 + (1 +\ldots+ N/2) = N/2 + (N/2)(N/2+1)/2 = N^2/8+ 3N/4$. We can repeat this argument with $\ell = N-2, N-4,\ldots,2$ to obtain

$$\frac{1}{8}\sum_{n \text{ even}}^{N} n^2 + \frac{3}{4}\sum_{n \text{ even}}^{N} n = \frac{1}{2}\sum_{m=1}^{N/2} m^2 + \frac{3}{2}\sum_{m=1}^{N/2} m$$

$$= \frac{1}{12}(2(N/2)^3 + 3(N/2)^2 + N/2) + \frac{3}{16}N(N+2)$$

$$= \frac{1}{48}(N^3+ 12N^2 + 20N).$$

Similarly, there are $(N-2)/2$ of the form $(N-1,N-1,2k)$; $(N-2)/2$ of the form $(N-1,N-2,2k-1)$; $(N-2)/2 - 1$ of the form $(N-1,N-3,2k)$, namely, for $k = 1,\ldots,(N-2)/2 - 1$; $(N-2)/2 - 2$ of the form $(N-1,N-4,2k-1)$, namely for $k = 2,\ldots,(N/2)/2 - 1$; and so on down to $1 = (N-2)/2 - (N/2 - 2)$ of the form $(N-1,N/2,N/2-1)$ for a total of $(N-2)/2 + (1 + \ldots + (N-2)/2)$. Repeating the argument for those of the form $(N-3,N-3,2k)$, etc., one sees that the grand total for $\ell = N-1,N-3,\ldots,3$ is the same as that obtained above but with N replaced by $N-2$. Hence, for N even the total is the first line of (29). But a reexamination of the last part of the combinatorial reasoning shows that we have established

that the number of non-zero (ℓ,m,n), $\ell \geq m \geq n$, with odd $\ell \leq N$, N odd, is precisely equal to the number of non-zero (ℓ,m,n), $\ell \geq m \geq n$, with <u>even</u> $\ell \leq N-1$. Using this fact we see that for N odd we get a total of twice the last mentioned number, once for N and once for N-1, or the second line of (29).

To complete our work it is only necessary to derive the formula (19) of Section 3. The limits in all the integrals in (5b) are $\xi = 0$, $\xi_0 = \pi$. The integral in the first term is thus -2, and the use of (17) accounts for the first term. A typical term in the integral of $\beta \cos \xi$ in the second term of (5b) becomes, when one sets $x = \cos \xi$,

$$-A_n \int_{-1}^{1} \sqrt{1-x^2}\, \frac{dP_n}{dx} \frac{x}{\sqrt{1-x^2}}\, dx = -A_n\left[\frac{n+1}{2n+1} + \frac{n}{2n+1}\right](1 - (-1)^{n+1})$$

$$= -(1 - (-1)^{n+1})A_n .$$

Here we have used the consequence

$$xdP_n/dx = [(n+1)/(2n+1)]dP_n/dx + [n/(2n+1)]dP_{n+1}/dx$$

of (20) and (23). For the next term of (19) we take the next two terms of (5b) and integrate the first by parts, noting that the integrated out terms disappear. Then the same device as used just now and (17) complete the term. The integral of $\beta \sin^2\xi \cos \xi$ in the last linear term becomes

$$-\sum_{n=1}^{s} A_n \int_{-1}^{1} P_n^1(1 - x^2)(x/\sqrt{1-x^2})dx$$

$$= \sum_{n=1}^{s} A_n \int_{-1}^{1} P_n(1 - 3x^2)dx = (4/5)A_2$$

since $1 - 3x^2 = 2P_2$, where (7a) and an integration by parts have been used.

The computation in (19) of the first two non-linear terms is clear since the substitution $x = \cos \xi$ turns the integrands, with the aid of (17), into inner products of β with itself and with ψ^*, respectively. The same devices convert the next non-linear integral, except for the factor K in (18), into

(29)

$$\int_{-1}^{1} \psi^* \beta \, \frac{x^2}{1-x^2} \, dx = \sum_{m,n=1}^{s} B_m^* A_n \int_{-1}^{1} x \, \frac{dP_m}{dx} \, x \, \frac{dP_n}{dx} \, dx$$

$$= \sum_{m,n=1}^{s} B_m^* A_n \int_{-1}^{1} \left(mP_m + \sum_{i=1}^{(m-1+p(m-1))/2} (4i-1-2p(m-1))P_{2i-2p(m-1)-1}\right)$$

$$\times \left(nP_n + \sum_{j=1}^{(n-1+p(n-1))/2} (4j-2p(n-1)-1)P_{2j-2p(n-1)-1}\right) dx \, ,$$

where (26) has been used, which gives the result indicated without the addend ν in parenthesis. The next non-linear term in (5b) becomes (up to a constant factor)

(30)

$$\int_{\pi}^{0} \psi^{*\prime} \beta \cos \xi \, d\xi = \int_{\pi}^{0} \left(\sum_{m=1}^{s} B_m^* (-\cot^2 \xi \, P_m^1 + m(m+1)\cot \xi \, P_m)\right)$$

$$\times \left(\sum_{n=1}^{s} A_n P_n^1\right) \sin \xi \, d\xi$$

$$= \int_{-1}^{1} \left(\sum_{m,n=1}^{s} B_m^* A_n \, x^2 \, \frac{dP_m}{dx} \, \frac{dP_n}{dx}\right) dx$$

$$- \int_{-1}^{1} \left(\sum_{m,n=1}^{s} B_m^* A_n \, m(m+1) \, x P_m \, \frac{dP_n}{dx}\right) dx \, .$$

Here the first equality results from (9b), (9c), and the resulting formula

$$\frac{d}{d\xi} P_m^1(\cos \xi) = -\cot \xi \, P_m^1(\cos \xi) + m(m+1)P_m(\cos \xi) \, .$$

But the first term of the second equality in (30) is

$$\int_{\pi}^{0} \psi^* \beta \cot \xi \cos \xi \, d\xi \, ,$$

as is seen from (29), and this yields the missing ν. The remaining term in (30) becomes

$$\sum_{m,n=1}^{s} B_n^* A_{n\,m(m+1)} \int_{-1}^{1} P_m \left(nP_n + \sum_{i=1}^{((n-1)+p(n-1))/2} (4i-2p(n-1)-1)P_{2i-p(n-1)-1} \right) dx$$

by (26), and this yields the next two terms of (19). Finally, from (24) we obtain

$$x^2 \frac{dP_n}{dx} = \frac{dP_n}{dx} + \frac{n(n+1)}{2n+1} (P_{n+1} - P_{n-1})$$

and this with (25) yields the final integral except for the indicated constant factor

$$-\int_{-1}^{1} x^2\beta^2 dx = -\int_{-1}^{1} x^2(1-x^2) \sum_{m,n=1}^{s} A_m A_n \frac{dP_m}{dx} \frac{dP_n}{dx} dx$$

$$= -\sum_{m,n=1}^{s} \int_{-1}^{1} \frac{m(m+1)}{2m+1} A_m A_n (P_{m-1} - P_{m+1}) \left(\frac{n(n+1)}{2n+1} (P_{n+1} - P_{n-1}) + \sum_{i=1}^{(n+p(n))/2} (4i-2p(n)-1)P_{2i-p(n)-1} \right) dx ,$$

which yields the final terms of (19).

7. Discussion

In this section we wish to take up a few points about comparison with different theories, other results and possible improvements or extensions.

First of all, in using E. Reissner's equations in small finite deflection form and retaining only the terms shown, we are adopting a quadratically non-linear theory (quadratic theory, for shortness), sometimes called a weakly non-linear theory. While this is admirably adapted to spectral (Galerkin) methods, one might very well suspect its accuracy or even relevance, in comparison with physical reality and with the full non-linear equations of E. Reissner, for the large deflections reported

in Section 5 in the post buckling range near $\rho^* = \rho_L^*$ and on the rising section of the pressure-deflection graph to the right. While conceding the physical unreality of the rising section of the graph, we feel there are some grounds for a cautious optimism about both comparisons. As far as the fully non-linear Reissner equations go, Mescall [8] has reported only insignificant differences between the predictions of that theory and the quadratic theory for large-deflection buckling of spherical caps, and that situation and ours are not so radically different. As far as physical reality goes, from the very beginnings of the type of approximate non-linear, in fact, quadratic plate and shell theories we are using, namely, the Föppl-von Kármán plate equations, comparisons with experiment have been remarkably accurate for deflections many times those for which the equations were originally estimated to be valid, e.g., tens of thicknesses versus one thickness for the F.-v.K. equations. Indeed, there is almost a metamathematical principle of unexpectedly large range of validity in many mathematical models in physics and technology. In the spherical case the shape of Figure 4 has not been observed experimentally to our knowledge, but that may well be due to the failure of the elastic stress-strain relations over portions of the shell at snap-through. In view of the differential-geometric plausibility of Figure 4 as discussed in Section 5, one can conceive of a carefully conducted experiment, possibly with certain constraints during buckling, using material (not metal) of exceptional elastic properties (linear elasticity through rather large strains), that would yield the shape of Figure 4.

It is clear that the spectral method will not work with the fully non-linear Reissner equations, but the pseudospectral method will. The pseudospectral method inserts expansions in complete function sets in a set of differential equations but, rather than reexpanding the equations,

simply demands that they be satisfied at a prescribed number of points. The advantages of that from the computing point of view is evident even for the cases when spectral methods are applicable. One suspects, however, a loss of accuracy per given number of modes vis-a-vis spectral methods in those cases.

Our computations have indicated that $a/h = 200$ is about the practical upper limit for our method with our present programs. However, it would be interesting to explore the possibility of applying fast transform methods as used by Orszag [9] in conjunction with spectral methods in fluid dynamics. His requirement of a finite expansion condition is precisely met here. The resulting shortening of the computation of the sums in (A') and (B') might well make possible many mode computations, necessary for $200 < a/h \leq 1000$, in less time than presently required for $a/h < 100$.

Finally, we show how to include the effect of small axisymmetric imperfections in Reissner's equations. The modified equations can be solved numerically by our codes after making the necessary obvious modifications. The result would be a modification of graphs to be Figures 2 and 3 near the origin (clearly one would need expanded deflection scales there). Unfortunately we did not possess the modified equations until the conclusion of the numerical work reported here, and we do not have numerical results for them. The important thing to notice is that the imperfection sensitivity (snap-through) analysis and deep post buckling analysis appear simultaneously as features of one non-linear large deflection analysis. There is ample precedent for this observation in plate and shallow shell analysis in the literature, but it bears reemphasizing.

The modified equations are obtained by adding the terms $P\Psi \cot \xi - \frac{1}{2} \rho a^2 P$ and $-P\beta \cot \xi$ to the right sides of (4a) and (4b), respectively, where

$$P = \sum_{n=1}^{s} \epsilon_n P_n^1(\cos \xi)$$

and ϵ_n, $1 \le n \le s$, is the (small) imperfection parameter for the n-th mode imperfection. These terms were suggested by equations (26-28) of [2]. They can be justified by inserting $\varphi_0 = \xi - P$ in equations (III) and (IV) of [12], getting $\sin \varphi_0 = \sin \xi - P \cos \xi$, $\cos \varphi_0 = \cos \xi + P \sin \xi$ there, and discarding the terms $P\beta\psi$, $\frac{1}{2} P\beta^2$ on the grounds that they are essentially cubic and, hence, negligible in a quadratic theory. The result is to add the terms

$$\frac{1}{K[n(n+1)-1-\nu]} \sum_{\ell,m=1}^{s} \left[\frac{(\ell,m,n)}{j_n}\right] \epsilon_\ell A_m, \quad -2 \sum_{\ell,m=1}^{s} \left[\frac{(\ell,m,n)}{j_n}\right] \epsilon_\ell B_m^* + \rho^* \epsilon_n ,$$

to the right side of the n-th equation of(A')and left side of the n-th equation of (B'), respectively.

The following simple analysis based on (A') and (B') shows the imperfection-sensitivity of the shell. Take s even, $A_n = B_n^* = 0$, $n = 1,\ldots,s-1$ and $|A_s|$ so small that its cubes are negligible. Eliminate B_s^* to obtain, after ignoring cubes and dividing by A_s,

$$\rho^* - 1 \cong - \frac{2}{K[s(s+1)-1-\nu] j_s} A_s . \tag{31}$$

This shows that ρ^* will decrease linearly from 1 for A_s small and positive, i.e., <u>inward</u> deflected poles, with the indicated .
If s is critical for a/h, i.e., (12) holds approximately then (31) becomes, by (12)

$$\rho^* - 1 \cong - \frac{(s,s,s)}{j_s} A_s \cong - \frac{\sqrt{3}}{\pi}(s + \tfrac{1}{2}) A_s \cong - \frac{\sqrt{3}}{\pi}(s + \tfrac{1}{2})v ,$$

on using the analysis in [15, p. 306] for large s, where v is the polar deflection in radii. Or one can write $(a/h)A_s \cong w$, the polar

deflection in thicknesses, to get Thompson's formula [13],

$$\rho^* - 1 \cong -[3(1-\nu^2)]^{\frac{1}{2}} \frac{\sqrt{3}}{\pi} \frac{w}{s+1} \quad .$$

8. Acknowledgements

This research was partially supported by the Air Force Office of Scientific Research under Grant No. AFOSR-71-2063.

Graduate School and University Center of
The City University of New York
33 West 42 Street
New York, N.Y. 10036

REFERENCES

[1] L. Bauer, E.L. Reiss, and H.B. Keller, Axisymmetric buckling of hollow spheres and hemispheres, Comm. Pure Appl. Math. 23(1970), 529-568.

[2] B. Budiansky, Buckling of clamped spherical shells, Proc. IUTAM Symp. Theory of Thin Elastic Shells (Delft, 1959), North-Holland, Amsterdam, 1960, 64-93.

[3] A.G. Gabril'iants and V.I. Feodos'ev, Axially-symmetric forms of equilibrium of an elastic spherical shell under uniformly distributed pressure, Prikl. Mat. Meh. 25(1961), 1629-1642. [Engl. Transl.- J. Appl. Math. Mech.].

[4] N.J. Hoff, The perplexing behavior of thin circular cylindrical shells in axial compression, Israel Journal of Technology, vol. 4 (1966), 1-28.

[5] J.W. Hutchinson, Imperfection sensitivity of externally pressurized shells, Trans. ASME Ser.E, J.Appl. Mech. 34(1967), 49-55.

[6] W.T. Koiter, The non-linear buckling problem of a complete spherical shell under uniform external pressure, Nederl. Akad. Wetensch. Proc. Ser. B, 72(1969), 41-123.

[7] W.T. Koiter, The effect of axisymmetric imperfections on the buckling of cylindrical shells under axial compression, Proc. Kon. Ned. Akad. Wet., B66(1963), 265.

[8] J. Mescall, Numerical solutions of non-linear equations for shells of revolution, AIAA J., vol 4(1966), 2041-2043.

[9] S.A. Orszag, Numerical simulation of incompressible flows within simple boundaries, I. Galerkin (spectral)representations,Stud. Appl. Math., vol. I(1971), 293-327.

[10] E. Polak, A globally conveiging secant method with applications to boundary value problems, SIAM J. Num. Anal., vol. 11(1974), 529-537.

[11] H.E. Rauch, Instability of thin-walled spherical structures under external pressure, Contributions to Analysis, ed. L.V. Ahlfors et al, Academic Press, New York, 1974.

[12] E. Reissner, On axisymmetricl deformations of thin shells of revolution, Proc. Symp. Appl. Math. 3(1950), 27-52.

[13] J.M.T.Thompson, The rotationally symmetric branching behavior of a complete spherical shell, Nederl. Akad. Wetensch. Proc. Ser. B 67 (1964), 295-311.

[14] Th. Von Kármán and H.-S. Tsien, The buckling of spherical shells by external pressure, J. Aeronaut. Sci. 7(1939), 43-50.

[15] E.T. Whittaker and G.N. Watson, "A Course of Modern Analysis," 4th ed. Cambridge Univ. Press, London and New York, 1927; Amer. Ed., Cambridge and New York, 1946.